Structures 69 (2024) 107581

Contents lists available at ScienceDirect

Structures

journal homepage: www.elsevier.com/locate/structures

Stiffness contribution and damage index of infills in steel frames considering moderate earthquake-induced damage

V. Nicoletti *, L. Tentella, S. Carbonari, F. Gara

Dept. of Construction, Civil Engineering and Architecture (DICEA), Università Politecnica delle Marche, Via Brecce Bianche 12, 60131 Ancona, Italy

ARTICLE INFO

Keywords:
Infilled steel structures
Damaged masonry infills
Impact load tests
Infill out-of-plane dynamics
Automatic 2-D element EMA
Infill in-plane stiffness reduction
Infill damage assessment
Infill damage index

ABSTRACT

This paper examines the contribution of infill wall stiffness to steel frame structures, taking into account moderate earthquake-induced damage and by introducing a damage index based on variations in the out-of-plane dynamic response of infills identified through experimental tests. The research involved an extensive laboratory experiment on a steel-concrete composite mock-up tested before, during, and after infill masonry wall damage. The study initially focuses on dynamic tests performed on infills to determine their out-of-plane dynamic behaviour, aiming to draw conclusions about their post-damage health condition and stability. An improved Matlab routine for the automatic identification of the experimental out-of-plane modal parameters of 2-D elements is developed; the tool is validated on a simple steel plate and then applied to track the experimental modal parameters of the mock-up infills during the progressive induced damage. Successively, the study examines how damage to the infill panels reduces their stiffness and strength. Two exponential equations are derived from the observation of the experimental outcomes. The former equation relates the infill stiffness reduction to a damage index of infill panels expressed in terms of modal frequency variation of their out-of-plane vibration modes. This equation can be used to obtain an estimation of the residual stiffness of infills to be used in the numerical modelling. The latter equation provides an indication about the total stiffness reduction of infilled structures if damage on infills is detected. The proposed strategy, supported by laboratory results, aids practitioners in evaluating the condition and usability of steel infilled structures following earthquakes.

1. Introduction

Masonry is undeniably the predominant material used for infill construction in framed buildings around the World [1]. Even though it is often associated with reinforced concrete structures, this type of infill is also commonly used in steel framed structures, especially those built before the implementation of modern seismic design standards [2–4]. Infill masonry walls significantly influence the dynamic and seismic behavior of steel framed buildings [5,6] because of their influential mass and stiffness contribution to the whole structural system [7,8]. This has a positive impact in terms of displacement reduction during the seismic shaking, but it is also associated to negative aspects, as the reduction of the fundamental period of the structure, with the relevant increase of the seismic forces [9], and the increase of the structure fragility in terms of damageability of non-structural members, which may be cause of buildings disuse after moderate earthquakes. Moreover, the non-symmetrical non-distributed presence of infills can alter the structural damage activation and can produce local collapse mechanisms in case of severe earthquakes [10]. Furthermore, infills contribute to increase the structural damping during earthquakes due to the activation of non-linear phenomena [11–13].

During the seismic shaking, damage to infills can lead to significant changes in the dynamic properties of the structure, and consequently in the structural response [14]. These changes are primarily due to a decrease in the infill stiffness contribution, since their mass remain almost unchanged. Besides, the reduction of the infill stiffness due to damage also compromises the Out-Of-Plane (OOP) stability of panels [15]. Dynamic identification techniques demonstrate to be promising for investigating infills damage [16]. Specifically, strategies involving the use of accelerometers fixed on infills for the acquisition of vibrations due to ambient noise or hammer impacts, are used by researchers with relevant Operational Modal Analysis (OMA) [17] and Experimental Modal Analysis (EMA) techniques [18,19]. The detection of damage can be achieved by comparing the dynamic parameters of the intact and damaged infill [20]. Some advancements in this procedure suggest the use of artificial intelligence algorithms to extract dynamic parameters,

* Corresponding author.
E-mail address: v.nicoletti@univpm.it (V. Nicoletti).

https://doi.org/10.1016/j.istruc.2024.107581
Received 13 August 2024; Received in revised form 6 October 2024; Accepted 14 October 2024
Available online 20 October 2024
2352-0124/© 2024 The Author(s). Published by Elsevier Ltd on behalf of Institution of Structural Engineers. This is an open access article under the CC BY-NC-ND license (http://creativecommons.org/licenses/by-nc-nd/4.0/).

aiming to make this process more adaptable for a continuous monitoring system [21]. Ultimately, tracking the changes in the infill dynamic parameters during damage serves as a valuable tool for the structural health monitoring [22]. Given the limited number of studies available in the literature dealing with vibration tests on infills and their use for the infill damage detection, the increase of researches discussing this topic and the relevant consequences on the structural response and on the infill stability after damage, are necessary.

This paper discusses about the stiffness contribution of infill walls in steel frame structures taking into account moderate earthquake-induced damage and by introducing a damage index based on modal parameters changes of their OOP response, the latter identified through Impact Load Tests (ILTs). In addition, some useful considerations on the infill health status and the residual safety level are provided as a function of the damage pattern. The research work is developed by using results of an extensive laboratory experimental campaign on a steel-concrete composite mock-up, which was tested before, during, and after the infill masonry wall damage. Many laboratory tests were performed and some results of the experimental campaign have already been published in [23], focusing on changes in the dynamics of the whole mock-up due to the progressive damage of infills. This work presents original results, mainly focusing on the dynamic tests performed on infills, which are used to identify their OOP dynamic behaviour at both undamaged and damaged conditions. ILTs on infills are well addressed in Section 2, after providing a summary of the whole experimental campaign and a detailed overview of the infill progressive damage produced during the experimental activity. Furthermore, an improved Matlab routine for the post processing of data recorded from dynamic tests on infills is proposed in Section 3. This routine allows for a substantial automatization of the modal identification process, which leads to obtain the OOP modal parameters of 2-D elements in a quick and simple manner. The improved routine is firstly validated with a simple small-size steel plate and then is adopted to identify the OOP vibration modes of the mock-up infills at different step of damage, the latter reported in Section 4. Section 5 is devoted to propose a strategy for addressing the evolution of the In-Plane (IP) infill stiffness contribution on the total stiffness of the steel mock-up as a function of the infill damage, expressed through a damage index evaluated on the basis of the OOP dynamics. Two equations are proposed in this sense. In addition, some useful considerations on the infill health status and on the residual safety level are provided, based on the experimental test results and on the proposed damage index. Results of this research may help practitioners to estimate the residual stiffening effect of damaged masonry partitions on steel frames through experimental approaches, as well as to qualitatively assess the infill residual safety level, contributing to the decision making process relevant to buildings usability during post-earthquake surveys.

2. Description of the laboratory experimental campaign

2.1. The whole experimental campaign

The laboratory experimental campaign included quasi-static and dynamic tests performed on a steel-concrete composite mock-up with masonry infills (Fig. 1b). The mock-up is 8.40 m long, 2.80 m wide, and 3.00 m high. The concrete slab is 0.12 m thick, casted on a collaborating steel sheet and connected to the steel frame with Nelson studs. Columns are fixed to the laboratory strong floor through post-tensioned anchor bolts. Concrete blocks are placed over the slab to simulate the mass of permanent and live loads. The infill masonry walls (W1 and W2) fill only one of the two longitudinal bays and are built with hollow clay bricks with bed and head mortar joints having thickness of about 1–1.5 cm. A thin gypsum plaster layer, with thickness of about 0.7 cm, is built over both sides of each wall. Quasi-static Cyclic Load Tests (CLTs) were executed by longitudinally pushing and pulling the whole mock-up with a hydraulic jack; the latter were designed to induce a step-by-step progressive IP damage to infills (simulating an earthquake damage scenario) while preserving the structural elements in the linear range.

Starting from the initial T0 configuration, CLTs foresaw 26 increasing displacement steps (from T1 to T26), associated to jack strokes ranging from 1 to 13 mm, corresponding to storey drifts from 0.3 to 4.0 ‰. In between, different types of dynamic tests on the infills and on the whole mock-up were performed to evaluate the response of the overall system and of its non-structural components to different level of infill damage. Specifically, Ambient Vibration Tests (AVTs), ILTs providing hammer blows, and Snap-Back Tests (SBTs) were performed on the mock-up, adopting the sensor layout reported in Fig. 1a. Results of these tests, combined with those of the quasi-static ones, gave useful information for the detection and tracking of damage to non-structural elements during and after seismic events by monitoring the global dynamics of the structure. A comprehensive discussion of tests and results may be found in [23]. Instead, the dynamic tests on both the undamaged and damaged infills are discussed in this work.

2.2. Summary of the progressive damage on infills and effects on the mock-up longitudinal stiffness

A brief summary of the main outcomes of the whole experimental campaign described in the previous section is here reported with only reference to damage on infills and their effect on the mock-up longitudinal stiffness. This summary is considered essential for the reader to correlate the damage on infills (experimentally investigated in this work) with the effects of this damage on the overall structural behaviour. During CLTs, the mock-up was longitudinally pushed and pulled at different displacement levels; hence both infills experienced the same IP

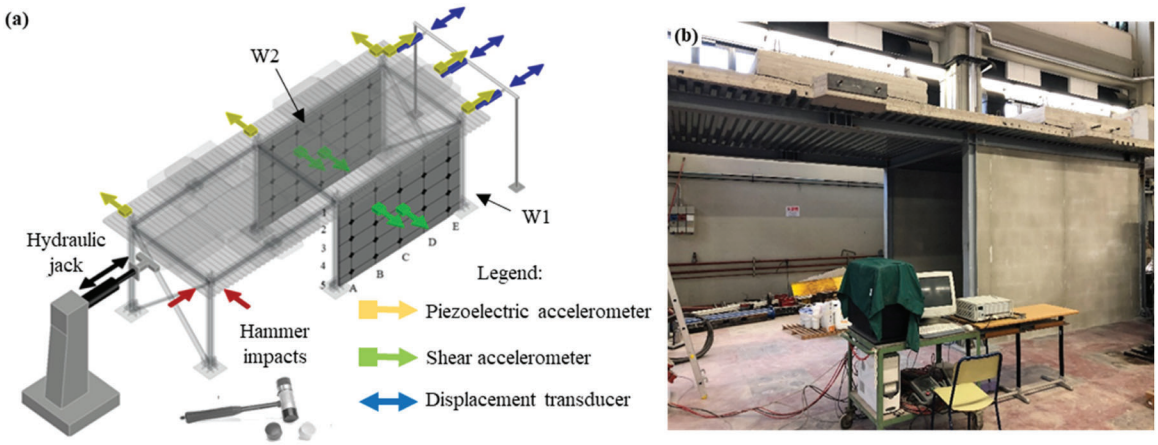

Fig. 1. Summary of the laboratory experimental campaign: (a) test set-up, (b) picture of the mock-up (before the infill damage).

displacement at the same time. Consequently, both infills suffered very similar progressive damage, which can be summarized as follows: at storey drift around 0.90 ‰ narrow and shallow diagonal cracks occurred on the upper corners; at 1.4 and 2.0 ‰ a horizontal crack along a bed joint and around the mid height of the panel occurred for W1 and W2, respectively; at the end of CLTs (drift around 4.0 ‰) both walls exhibited similar shear failure mechanisms and were completely cracked (Fig. 2c). A schematic representation of the infill progressive damage is illustrated in Fig. 2a. The relevant mock-up hysteretic cycles (depicted in Fig. 2b) show sudden drops in correspondence with storey drifts between 1.4 and 2.0 ‰ in both push and pull directions. This sharp decrease is caused by a significant damage to both infills, resulting in a reduction of the IP stiffness and strength of the infill walls. Indeed, as previously stated, the steel frame always remain in its elastic state. After this drop, the IP strength of the infills continue to increase, while the longitudinal secant stiffness decreases, approaching the static stiffness of the bare mock-up (represented with a dashed grey line). Values of the infilled mock-up longitudinal secant stiffnesses during the main steps of the infill damage are listed in Table 1, flanked to the relevant storey drift, the CLT step, and a brief damage description. It is worth observing that the maximum longitudinal secant stiffness is not achieved at the beginning, but when the drift reached 0.35 ‰, meaning that small IP displacements are required to fill the gap between the infill and the steel frame to activate infill resisting mechanisms, obviously without producing damage to infills. Moreover, when infills are completely damaged, their contribution to the overall stiffness of the mock-up is low but still significant, being greater than that of the bare frame.

Table 1
Evolution of the mock-up longitudinal secant stiffness as infill damage progress.

Storey drift [‰]	Mock-up longitudinal secant stiffness [kN/mm]	CLT step	Damage on infills
0.35	105	T4	No damage (filling the gap between steel frame – infills)
0.90	87	T9	Narrow and shallow diagonal cracks on the upper corners
1.40	64	T12	Formation of horizontal cracks in W1
2.00	44	T14	Formation of horizontal cracks in W2
4.00	20	T26	Development of diagonal cracks and brick spalling

2.3. Dynamic tests on infills

ILTs on both infills were performed with the target of identifying their OOP dynamic behaviour. ILTs consist in exciting the panel with hammer blows orthogonally applied to the wall plane, and in recording the time history of the impulse and that of the produced accelerations in the same direction. The panels were divided with a standard grid of 25 points, dimensioned according to the infill heigh and length, in order to be able to experimentally investigate relatively high frequencies (Fig. 3). Two shear accelerometers were placed in different positions on each wall to provide redundancy and ensure the identification of a large number of modes, including those with no modal displacement at the sensor location. The position of the accelerometers (B2 and C3 grid points) was decided based on optimal sensor placement analysis results

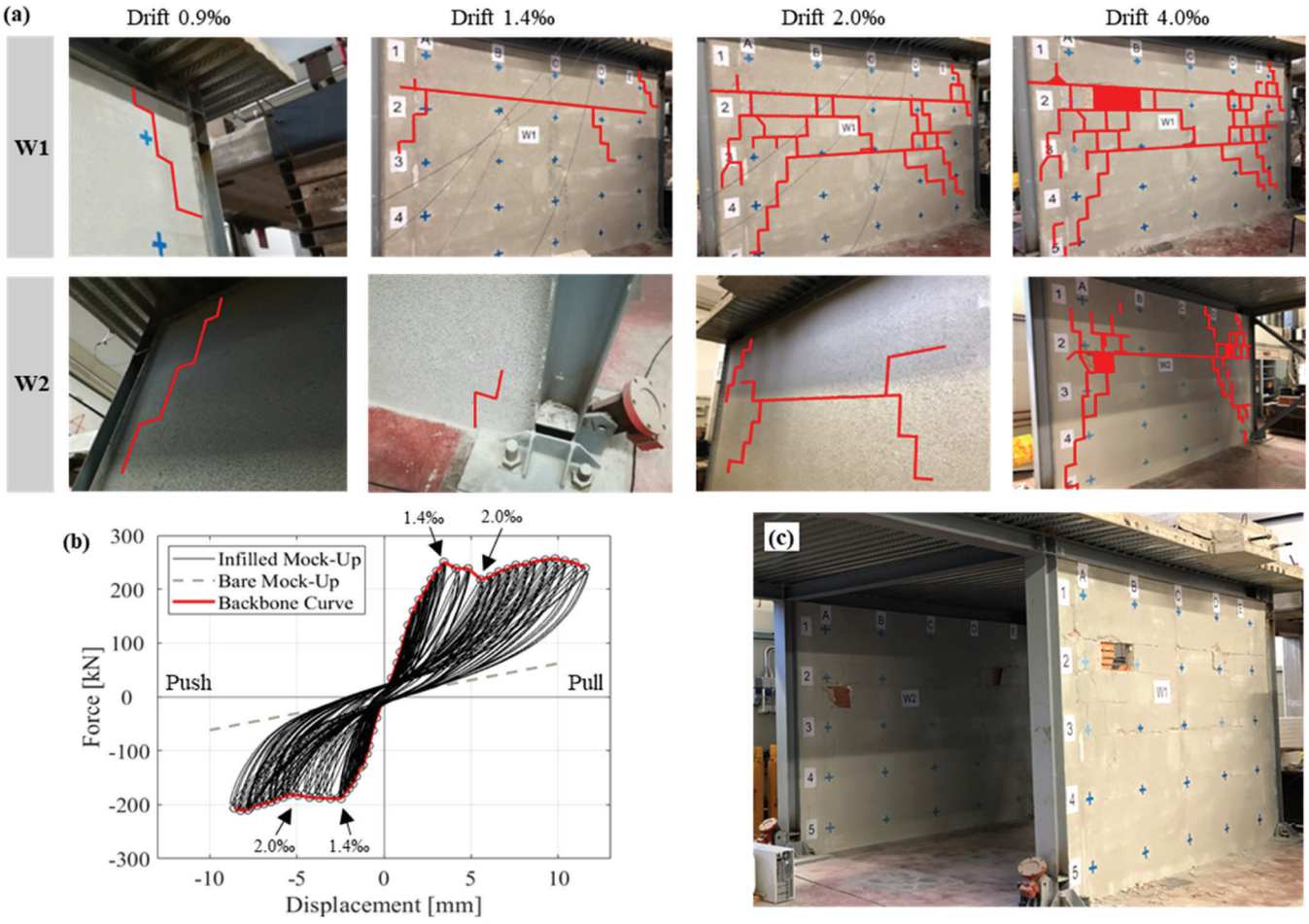

Fig. 2. Infill progressive damage: (a) pictures of W1 and W2 during the progressive damage, (b) mock-up hysteretic cycles, (c) picture of the mock-up (end of the cyclic tests).

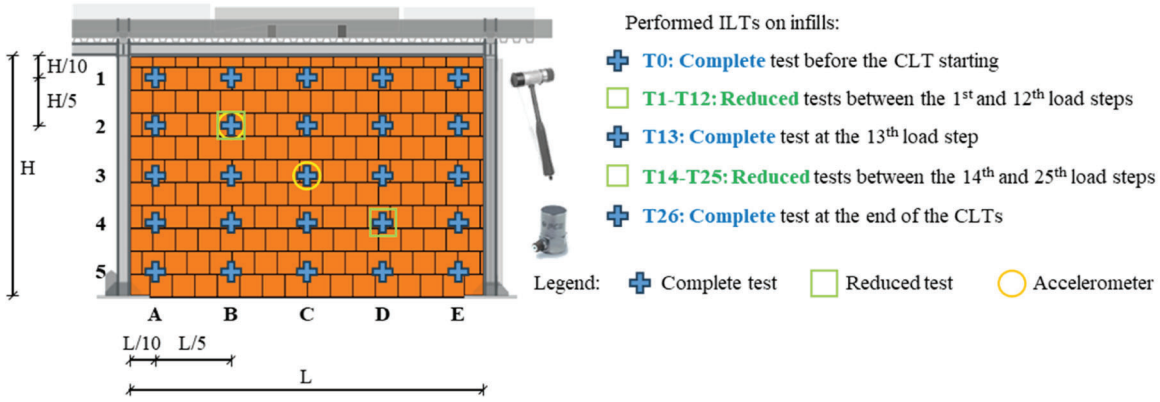

Fig. 3. Infill ILT set-up and performed tests.

and taking into account a high number of OOP vibration modes of the infills. Tests were executed by providing hammer blows to each of the 25 grid points while retaining the accelerometers in the same positions. The test procedure was proposed by the authors in [18], where the reader may find further details. Then, identification of the OOP modal parameters was performed by using the Line Fit method [24] and by adopting a suitable developed automatic procedure that will be discussed in the next section.

ILTs on infills were executed many times: complete dynamic tests (i.e., by applying hammer blows on all grid points) were performed on both walls before (T0), in the middle (T13), and at the end of CLTs (T26). Instead, reduced ILTs were performed during all other phases of the CLTs, by applying hammer blows only in two grid points (B2 and D5). This was necessary to reduce the testing time assuring an accurate frequency tracking during the progressive damage of infills. On the contrary, the complete ILTs, which also allows the mode shape identification to be performed, are executed in crucial steps of the test, assuring the modal tracking. This strategy is of paramount importance in cases when vibration modes change their frequency order, and performing frequency tracking without mode shape tracking could be misleading. A summary of the performed ILTs on both infill walls is reported in Fig. 3.

3. An improved Matlab routine for the automatic dynamic identification of OOP modes of infill walls

The EMA of infills is performed by considering the Single-Input Single-Output (SISO) strategy and by using the Line Fit method [25]. SISO means that the identification is done by considering one input and the relevant one output at a time to build the relevant Frequency Response Function (FRF). The modal analysis foresees the definition of a frequency interval around each FRF peak that is used to perform the Line Fit method; for the case at hand, this must be the same for all the 25 FRFs. However, a great drawback of this procedure is that results are sensibly influenced by the definition of the interval and no general recommendations can be provided for its definition, since each structure may be characterised by very different FRFs. Consequently, the user must try many times to find the best interval around each peak, and often this is extremely time consuming. In order to overcome above issues, an improved procedure for the automatic definition of the optimal frequency interval and its quantitative assessment in well identifying the corresponding modal parameters, is proposed and implemented in Matlab environment.

The improved procedure for the automatic dynamic identification is schematized in Fig. 4. Three main parts are the kernel of the automated process: step (3), step (5) and the combination of step (6) to (10). The former foresees the development of a numerical model of the tested infill that is required for obtaining benchmark data on infill OOP mode shapes. This is done with the support of a commercial software (CSI SAP 2000) in an automatic manner. Indeed, once the geometry of the wall is defined in step (2), the Matlab-SAP Toolbox [26] routine automatically generates the relevant numerical model, by considering a 4-edge fixed plate with homogeneous, elastic, and isotropic material, and performs the modal analysis. The numerical modal displacements of the 25 points corresponding to the tested grid points during ILTs are collected in vectors and analysed to automatically determine the mode typology. In fact, each vibration mode is named and classified with a couple of number (n, m), which represents the number of semi-waves characterizing the mode shape along the horizontal (m) and vertical (n) alignments, respectively. The numerical modes are automatically named by the routine by analysing the number of sign reversal on the displacement vectors of the vertical and horizontal wall lines. For example, in Fig. 4 the first five numerical modes of a typical wall and their automatic naming are shown.

A subsequent improvement is achieved in step 5, where peaks of the mean FRF are automatically detected. These peaks can represent possible infill OOP modes and they need to be considered in the identification procedure. However, the major advancement is inherent to the automatic determination of the best frequency interval to be used for obtaining the infill modal parameters, and in the automatic selection of the best solution. This is achieved by adopting a procedure that foresees the iterative variation of the considered frequency interval across each FRF peak until the identified mode shape closely resembles the ideal numerical one obtained in step (3). More specifically, for each peak of each of the 25 FRFs, four starting frequency intervals centred around the frequency peak (i.e., $\pm$ 2.5, $\pm$ 5, $\pm$ 7.5, $\pm$ 10 Hz) are used in the Line Fit method. Then, for each starting frequency interval, 35 different ranges are taken into account, as depicted in Fig. 4, for a total of 140 tested frequency ranges used for identifying each FRF peak. The improved Matlab routine applies the Line Fit method considering all these frequency ranges and saves all the relevant results, which are compared with the numerical mode shapes by calculating the Modal Assurance Criterion (MAC) index [27]. In this way, the best experimental solution among the 140 is automatically recognised and named. However, a MAC lower threshold (MAC_{min}) is set to ensure that the considered FRF peak represents a global mode of the infill. In case the MAC from all the 140 solutions does not exceed this lower threshold, the mode is neglected. The authors suggestion is to adopt a $MAC_{min} \geq 0.70$ to reach a trade-off between a good dynamic identification and the possibility to find as much vibration modes as possible.

The improved Matlab routine is validated for the dynamic identification of the OOP modes of a very simple steel plate with 40 $\times$ 30 cm plan dimensions and 2 mm of thickness (Fig. 5a). The plate is fixed on the four edges by using steel stripes and clamps. The proposed test typology described in Section 2.3 is herein repeated, creating a 5 $\times$ 5 test grid on the plate. In this case, a smaller instrumented hammer and two

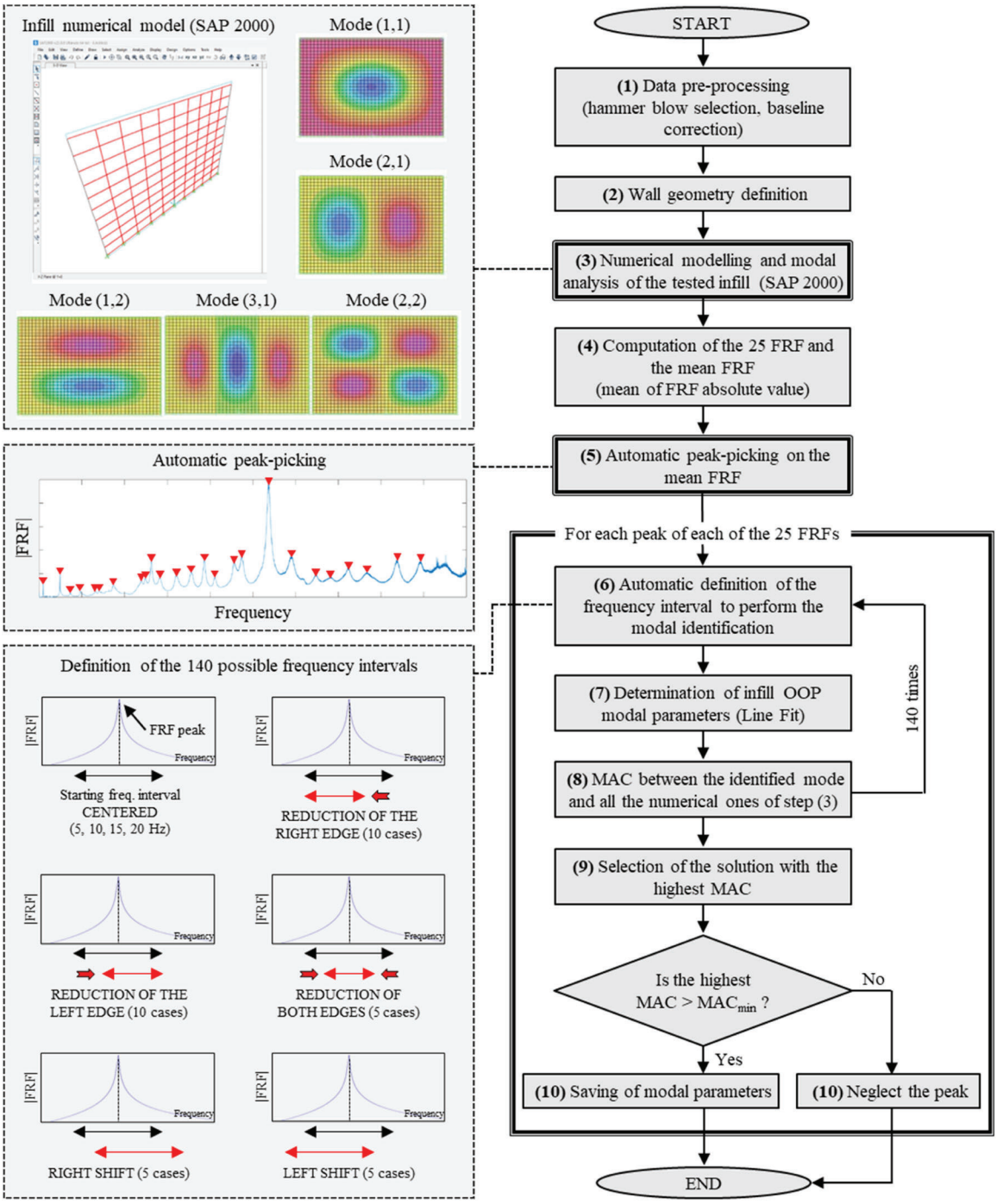

Fig. 4. Flowchart of the improved Matlab routine for the automatic EMA of infill walls.

piezoelectric accelerometers with a very small mass and high frequency range were employed (Fig. 5b). The plate was tested in two different configurations: (i) clamped on a stiff steel beams fixed on the floor (Fig. 5c), and (ii) suspended on the four corners (Fig. 5d). Results of EMA by using the improved Matlab routine are reported in Fig. 5f, together with the mean FRF of the accelerometer placed in B2 for the suspended plate, as an example (Fig. 5e). The numerical mode shapes obtained at step (3) are reported for completeness since they are not commonly displayed by the routine during its use. It is worth noting that at most 25 modes are considered by the software because this is the highest number of modes that can be identified with the proposed grid (25 test points) without falling into spatial aliasing problems. The dynamic identification of the steel plate is performed by setting a frequency upper limit of 2000 Hz. Therefore, a smaller number of experimental modes than the numerical ideal ones is identified in the frequency range 0 – 2000 Hz. More specifically, 21 modes for the case of fixed plate on the floor and 18 modes for the suspended case are found and reported in Fig. 5f. Apart from the second and third modes and the very higher ones, the plate in the suspended configuration lead to obtain more refined mode shapes, much similar to the numerical ideal ones, as demonstrated by the high MAC values. Among the first 12 modes, 8 modes for the suspended plate are characterised by MAC greater than 0.85, while for the plate fixed on the floor only 4. Nevertheless, for both configurations, the improved developed Matlab routine proved to be very effective in the automatic identification of almost all possible vibration modes of the steel plate in a straightforward and quick manner.

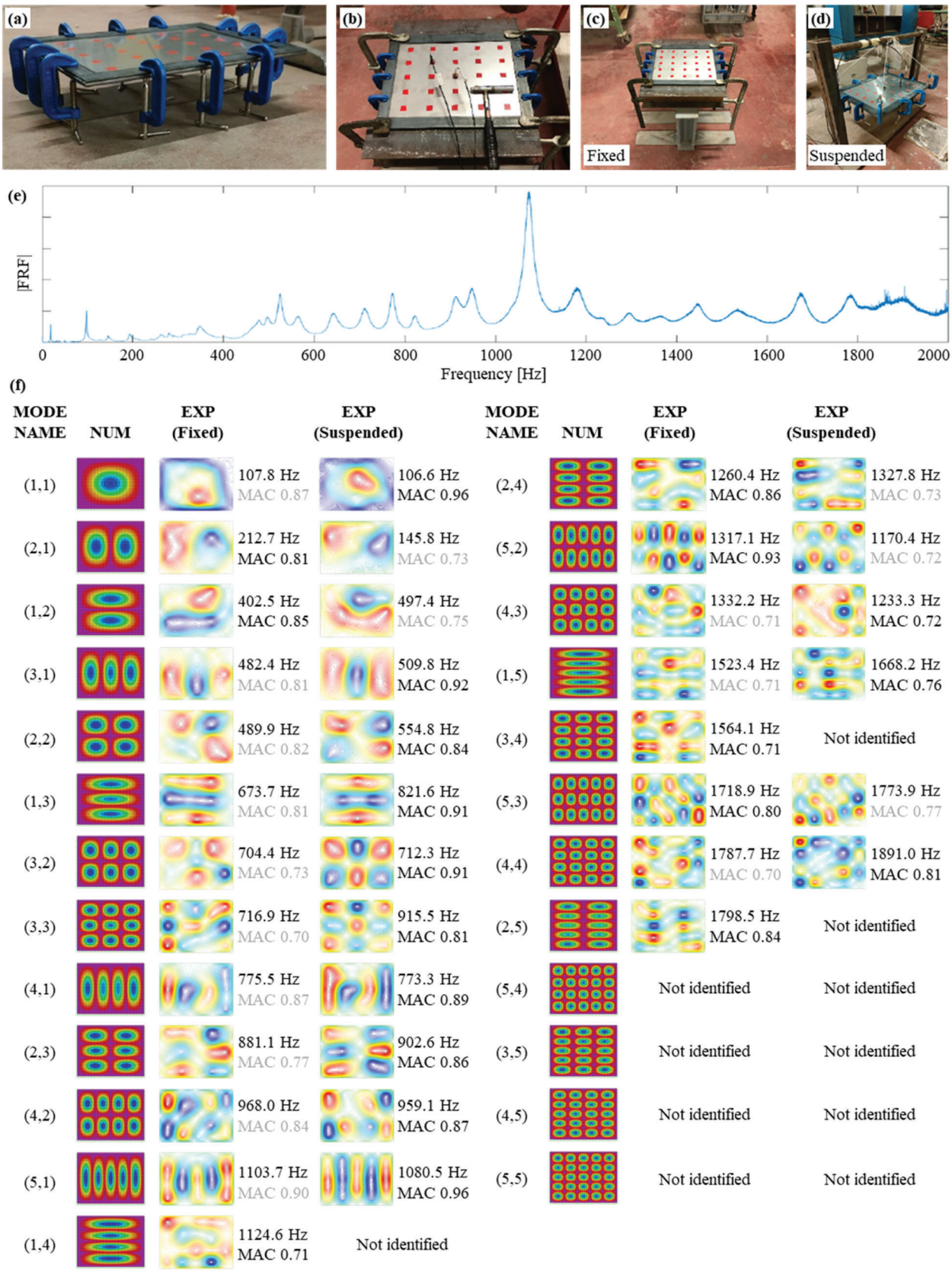

Fig. 5. Validation of the improved Matlab routine: (a) tested steel plate, (b) ILT set-up, (c) test configurations fixed on the floor and (d) suspended, (e) mean FRF for the accelerometer in B2 for the suspended plate, (f) EMA results.

4. Evolution of infill modal parameters during damage increase

The improved Matlab routine proposed in Section 3 is here used to identify the OOP vibration modes of the infill masonry walls dynamically tested during the laboratory experimental campaign described in Section 2. In particular, the automatic routine is used to find the OOP modes of both walls when the complete ILTs are performed, namely, before (T0), in the middle (T13), and at the end of CLTs (T26). In between these tests, the frequencies of the OOP modes of infills are identified by simply using the peak picking method on the relevant FRF, without the need of complex modal identification procedures. Obviously, this is possible because the modal tracking is based on the three detailed modal identifications performed in key phases of the experimental campaign and that provide fundamental information about the evolution of the OOP mode shapes of infills.

The OOP frequencies of both walls identified with the improved Matlab routine before the damage (T0) are collected in Table 2. For each wall, the same 13 modes are clearly found in the frequency range 17.3 – 212.5 Hz. As expected, the OOP behaviour of both walls is very similar because the infills were built with the same material and construction technique. However, frequencies of W2 are slightly higher than W1, denoting a slightly stiffer wall. This could be due to small differences in the plaster layer thicknesses, as well as to different head and bed mortar joint filling. Nevertheless, it is interesting to observe that, despite the infill construction was made by workers without using prefabrication and standardization, the mechanical properties of the two walls are quite similar, meaning that the considerations arising from this work can be generalised to other infill masonry walls with similar features. The mode shapes of W1 are shown in Fig. 6a, whereas those of W2 are omitted for the sake of brevity and because they are almost identical to those of W1.

The frequencies of the first four modes of each wall are traced during the CLTs. The first four modes were selected as they are sufficient for quickly and effectively analysing and identifying the progressive damage of the infills. The evolution of the frequencies of these four modes is illustrated in Fig. 7 as a function of the storey drift measured during the 26 CLT steps. Dynamic parameters identified from complete ILTs are highlighted with yellow rumbles. The storey drifts in which a crucial damage of infills was observed (both visually and with the support of the hysteresis cycles of Fig. 2b) are represented with dashed lines. The first cracks at corners appear around 0.9 ‰ of storey drift; however almost all frequencies start to decrease since the beginning of ILTs and no evident sharp decrease is detectable at that drift. On the contrary, in correspondence of the main damage (1.4 ‰ for W1 and 2.0 ‰ for W2), a noticeable frequency decrease is observed, especially for the higher modes (the 3rd and the 4th).

The mode shapes of the four traced modes identified in correspondence of the two complete dynamic identification during the infill damage (T13 and T26) are compared with the relevant ones obtained at the beginning (T0). The comparison is performed with MAC indexes (Table 3). The MAC reduces as the infill damage increases, and the greater reductions are for the 3rd and 4th modes. Indeed, the mode shapes of higher modes are characterized by a higher number of semi-waves; thus, the local variation of mechanical properties due to damage is probably responsible for a significant variation of mode shapes characterised by a high number of semi-waves, which reflects on the MAC index. The mode shapes of both walls at the end of CLTs are reported for comparison in Fig. 6b,c.

Table 2
Identified OOP modes of infills before the damage (T0).

Mode name	Frequency [Hz]	
	W1	W2
1,1	17.30	18.10
2,1	31.60	32.15
1,2	49.00	49.97
3,1	49.40	50.50
2,2	63.88	64.50
4,1	66.50	68.10
3,2	85.98	82.67
2,3	105.30	107.13
4,2	113.75	127.30
5,1	120.71	119.90
3,3	131.19	133.20
5,2	143.93	155.90
5,3	198.85	212.50

5. Qualitative assessment of the infill residual safety level and contribution on the lateral stiffness of steel frames

Changes in infill dynamics can reveal damage, indicating the infill's health and stability, and providing information on the residual safety level. The damage level can result from visual inspections or can be determined by performing ILTs on infills before and after exceptional events (e.g., earthquakes, blasts, etc.). The latter approach is more reliable than visual inspection alone, and can be used in conjunction with it to support the inspector's judgment. Observing the frequency evolutions of Fig. 7 and having in mind the infill crack patterns of Fig. 2a, an effort is done to correlate the frequency drop with the detected damage. At very small drifts (between 0.1 - 0.4 ‰), the degradation of the infill panel-frame interface causes a slight decrease in the OOP frequencies (an average of 5 % on all frequencies), while an increase in both strength and stiffness is observed. The infills do not experience significant damage and the OOP frequency change is probably related to a degradation of the boundary conditions that are necessary for the development of the panel's IP resisting mechanism. Conversely, at higher drifts, the formation of horizontal cracks initially (drifts about 1.4 – 2.0 ‰), and diagonal cracks subsequently (drifts up to 4.0 ‰), results in a significant frequency and MAC reduction. Specifically, frequencies decrease on average of about 17 % due to horizontal cracks formation, and 35 % at the end, while MAC of about 0.80 and 0.69 are found, respectively. It is worth noting that MAC reductions are calculated by only considering higher modes (the 3rd and 4th) because the first two modes remain almost unchanged for all infill damage steps. For the case at hand, an average reduction of about 17 % of the frequency, obtained for a mean drift of about 1.7 ‰, corresponds to an infill damage level that probably compromises the occupant safety. Indeed, diagonal and horizontal cracks occurred, and the infill stability due to aftershocks may be compromised, although tests revealed that the infill IP strength continues to increase by increasing the drift (see the hysteretic cycles of Fig. 2b).

To provide a more general discussion, a non-dimensional Infill Damage Index (*IDI*) is introduced, defined as the ratio between the frequency of the *i*-th OOP vibration mode (f_i) identified after the exceptional event (in this laboratory example, after each load step) and the relevant one identified at the undamaged condition (f_0, before the exceptional event).

$$IDI = \frac{f_i}{f_0} \tag{1}$$

Fig. 8 depicts the *IDI* evolutions for each of the four modes of each tested wall, together with the mean value calculated for the four modes (IDI_{av}). Observing the latter is evident how the major reductions of this index are detected in proximity of the main damage activation of each wall. At the activation of the main damage (horizontal cracks), W1 has a IDI_{av} of 0.86, while W2 of 0.84. At the end of CLTs, both walls are characterized by a IDI_{av} around 0.65, meaning that, when infills are completely damaged, their mean frequency decay is about 35 % with respect to the beginning. This is a benchmark data that can be used in the practice to assess on site infill walls with similar features of those tested in this experimentation. Nevertheless, other experiments should be collected to have a more confirmed number.

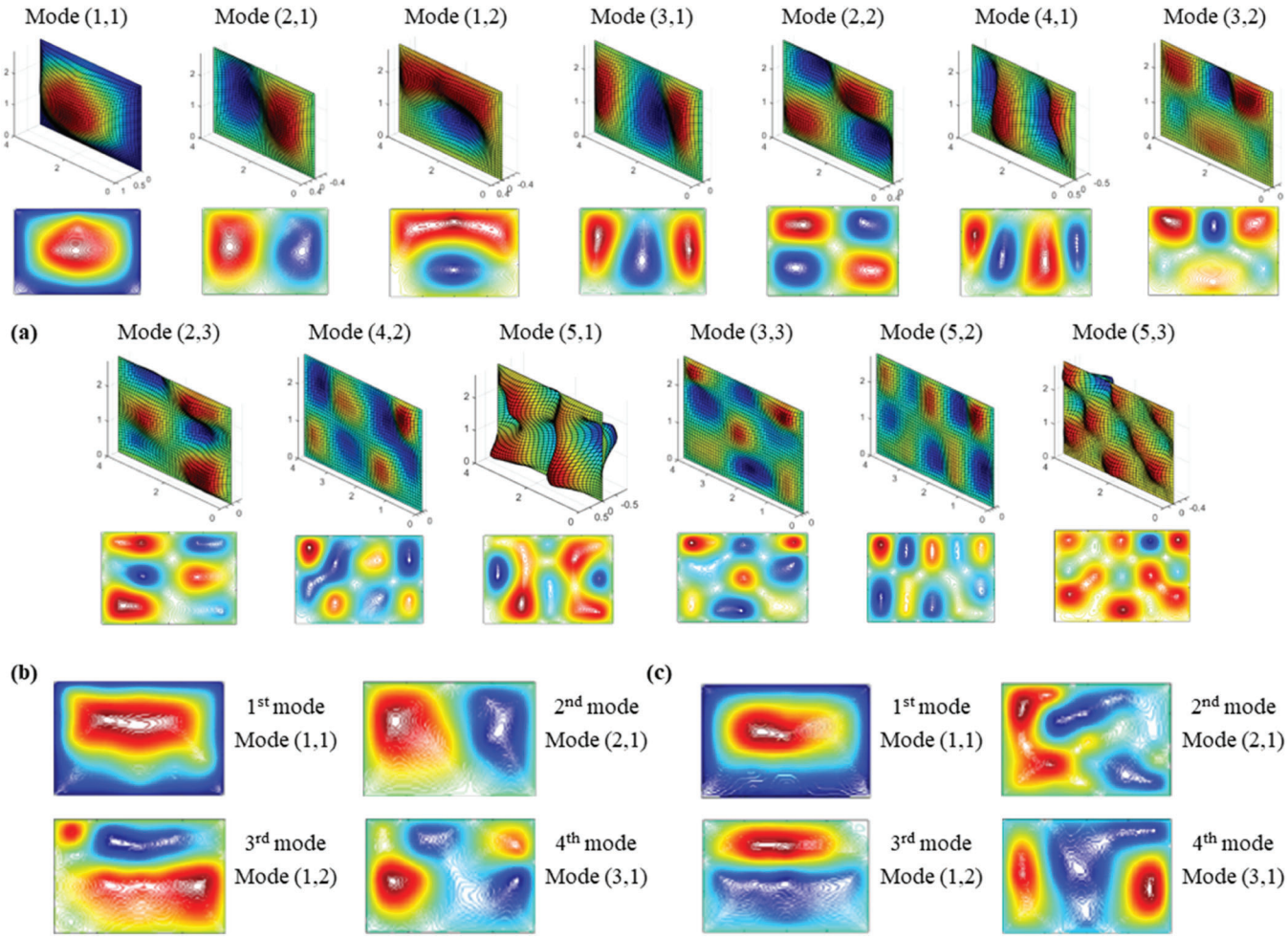

Fig. 6. Mode shapes of infill masonry walls: (a) infill W1 before the damage (T0), (b) W1 and (c) W2 at the end of cyclic tests (T26).

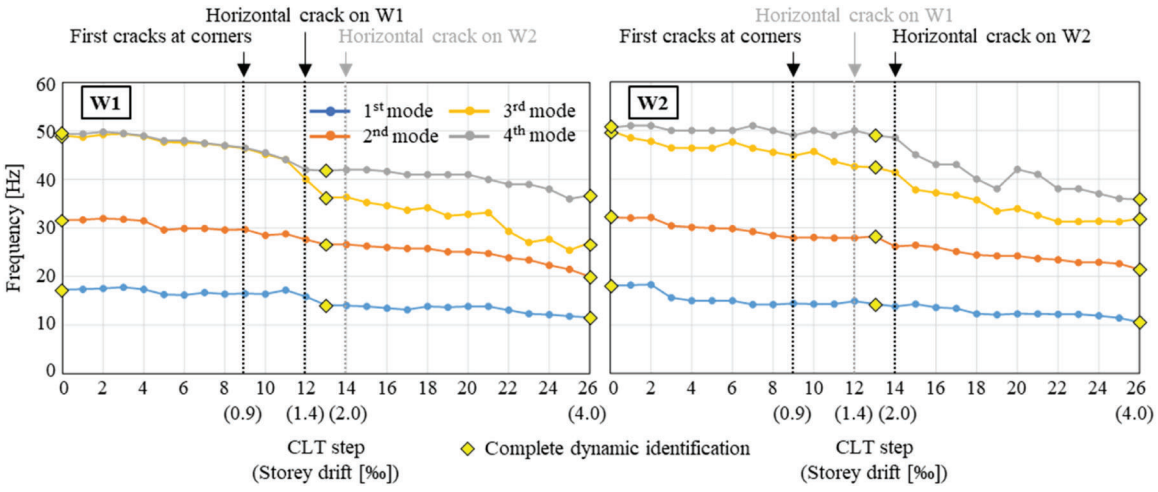

Fig. 7. Frequency evolutions of the first four OOP infill vibration modes during the progressive damage of both walls.

The outcomes of this laboratory experimentation are also used for assessing the infill stiffness contribution to steel frame structures in order to provide benchmark results that can be used in the modelling and analysis of steel structures when infill masonry walls are used as non-structural components. Moreover, the reduction of the stiffness (and strength) due to the panels damage is investigated as well. At first, the Infill Stiffness Reduction (*ISR*) non-dimensional parameter is defined to consider the IP stiffness decrease of these non-structural elements due to their damage. This is defined as the ratio between the actual value of the IP wall stiffness ($k_{w,j}$, determined at each j-th load step in this case study) and the relevant maximum value ($k_{w,max}$), which is obtained at T4 step (as reported in Table 1) because slight longitudinal displacements of the whole structure are required to activate infill resistant mechanisms.

Table 3
MAC between the results before CLTs (T0) and at 13th step (T13) and after the CLTs (T26).

Mode number	Mode name	MAC			
		W1		W2	
		T0 vs T13	T0 vs T26	T0 vs T13	T0 vs T26
1st	1,1	0.98	0.94	0.97	0.95
2nd	2,1	0.92	0.90	0.96	0.93
3rd	1,2	0.87	0.81	0.79	0.68
4th	3,1	0.81	0.63	0.72	0.70

$$ISR = \frac{k_{w,j}}{k_{w,\max}} \tag{2}$$

It is worth underling that k_w of each panel is obtained by subtracting the longitudinal stiffness of the bare steel frame (k_b) to the total longitudinal stiffness of the mock-up (k_T), the latter obtained from the hysteretic cycles of Fig. 2b, and dividing by two; thus, it represents the IP stiffness of each infill. The *ISR* of W1 is related to the IDI_{av} for each CLT step. Results are plotted in Fig. 9a, where it is possible to note that the maximum contribution in terms of IP stiffness (*ISR* = 1) of each infill is reached for a IDI_{av} lower than 1 (around 0.96), for the reasons previously discussed.

The evolution of *ISR* with the IDI_{av} is characterised by an exponential trend, which can be fitted by the following exponential function:

$$ISR = 0.0021e^{(6.47IDIav)} \tag{3}$$

The latter can be used to reasonably obtain an estimate of the IP stiffness reduction of the infill by calculating its IDI_{av}, namely, by executing a ILT campaign on the damaged infill (obviously, owing the ILT data on the undamaged condition).

It is also interesting to investigate the effects of the infill damage on k_T in order to gain useful information on how a certain damage level on these non-structural components can affect the total stiffness of an infilled steel frame structure. The total stiffness is normalized with respect to k_b in order to obtain a direct indication about the infill stiffness contribution on the total stiffness. The ratio k_T/k_b can be related to IDI_{av} calculated on both infills during the CLTs, and reported in Fig. 9b. As before, the maximum longitudinal stiffness is reached at T4 step and it is about 17 times the bare frame. The ratio k_T/k_b decreases by decreasing the IDI_{av} (namely, by increasing the infill damage) following an exponential trend, which can be fitted with:

$$\frac{k_T}{k_b} = 0.0084e^{(5.54IDIav)} \tag{4}$$

Once again, the equation can be used to reasonably estimate the stiffness loss due to the infill damage starting from ILTs aimed to identify the OOP infill dynamics. Eqs. 3 and 4 can be used for the determination of the stiffness parameter evolution of infill masonry walls with similar characteristics of those tested in this work, namely light infills with similar aspect ratios and thicknesses. However, a wider generalization of the expressions necessarily requires further validations. It is worth observing that the approach adopted to extract these correlations from experimental data (step-wise IP cyclic tests on infills combined with ILTs) is general and can be used to find other correlations usable for many types of infill walls, made by masonry or by other materials. Further researches are welcomed in this sense.

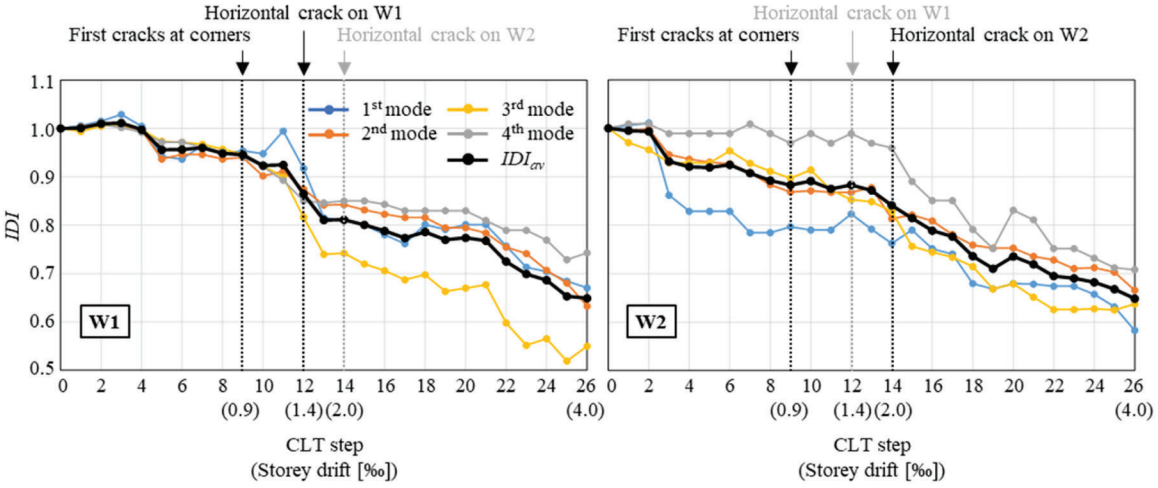

Fig. 8. *IDI* and its mean value (IDI_{av}) evolutions during the progressive damage of both walls.

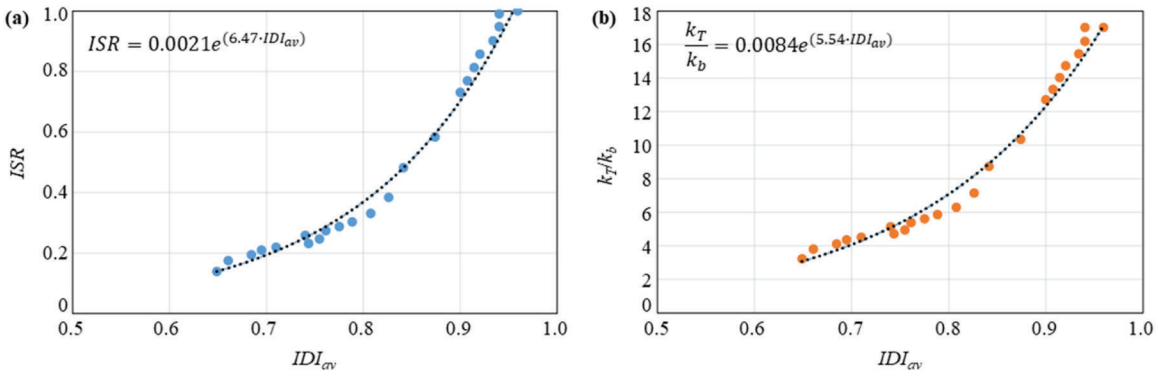

Fig. 9. Infill stiffness evolution and correlation with the infill damage: (a) *ISR* vs IDI_{av}, (b) k_T/k_b ratio vs IDI_{av}.

6. Conclusions

This paper examined the stiffness contribution of infill masonry walls in steel frame structures taking into account moderate earthquake-induced damage and by introducing a damage index based on modal parameters changes of their out-of-plane response identified through experimental tests. The research is based on an extensive laboratory experimental campaign conducted on a steel-concrete composite mock-up, tested before, during, and after damage to the infills produced by cyclic loads acting in the infill plane. The study primarily focuses on dynamic impact load tests performed on the infills to determine their out-of-plane dynamic behaviour, aiming at defining a damage index to correlate the observed damage with the stiffness reduction and with the residual safety of walls, the latter expressed from a qualitative point of view.

Firstly, an improved Matlab routine for the automatic out-of-plane dynamic identification of plate elements is proposed, capable of identifying the best frequency interval around each peak of the frequency response functions to be used in the Line Fit identification method. The improved Matlab routine is validated on a simple steel plate, demonstrating high effectiveness in automatically identifying many vibration modes in a straightforward and rapid manner. The tool is then used to identify the out-of-plane vibration modes of the mock-up infills during their progressive damage, in combination with the classic peak-picking method. Focusing on the first four modes of each infill, results demonstrate that both frequencies and MAC indexes decrease as the damage progresses, with a more pronounced decrease for the infill higher modes.

Results from the laboratory experimentation are then used to assess the contribution of infill stiffness to steel frame structures as a function of a proposed infill damage index, defined as the ratio of the out-of-plane frequency normalised by the relevant frequency at undamaged stage, averaged over the first four modes. Exponential correlations are found between the defined infill damage index and the stiffness reduction of infill and mock-up. In addition, qualitative considerations on the residual safety level of infills as a function of the damage are provided as well. In detail, for the tested mock-up it was observed that a drift of about 1.7 ‰ produces a frequency drop of about 17 % with respect to the undamaged state, corresponding to a critical safety condition because of the activation of both longitudinal and diagonal cracks that may compromise the infill stability in case of aftershocks. For a 4 ‰ of storey drift, a frequency drop of about 35 % is observed, as well as an increase of the crack patterns and crack thicknesses.

The experimental results support the effectiveness of non-destructive impact load tests on infills for addressing the damage level after exceptional events (e.g., earthquakes, blasts, etc.). Providing that the out-of-plane dynamics of typological partitions is known, tests can be adopted to derive an effective damage index through which the infill stiffness loss can be estimated, as well as useful information about the residual safety level can be derived. The results achieved in this work may support practitioners in evaluating the health condition and usability of infilled steel structures following exceptional events. Furthermore, impact load tests on infills could be used also as a non-destructive test for supporting their residual safety level assessment, giving an useful support to the post-event visual inspection outcomes.

CRediT authorship contribution statement

Vanni Nicoletti: Writing – original draft, Visualization, Software, Methodology, Investigation, Formal analysis, Data curation, Conceptualization. **Luca Tentella:** Writing – original draft, Visualization, Data curation. **Sandro Carbonari:** Writing – review & editing, Supervision, Investigation. **Fabrizio Gara:** Writing – review & editing, Supervision, Project administration, Investigation, Conceptualization.

Declaration of Competing Interest

The authors declare that they have no known competing financial interests or personal relationships that could have appeared to influence the work reported in this paper.

Acknowledgements

This work is developed within the research project DPC-ReLUIS entitled: WP12 – Standard contributions relating to civil and industrial steel and steel-concrete composite constructions (2022 – 2024).

References

[1] Nicoletti V, Arezzo D, Carbonari S, Gara F. Dynamic monitoring of buildings as a diagnostic tool during construction phases. J Build Eng 2022;vol. 46:103764. https://doi.org/10.1016/j.jobe.2021.103764.
[2] Di Sarno L, et al. Assessment of existing steel frames: numerical study, pseudo-dynamic testing and influence of masonry infills. J Constr Steel Res 2021;vol. 185: 106873. https://doi.org/10.1016/j.jcsr.2021.106873.
[3] Yu Q-Q, Wu J-Y, Gu X-L, Wang L. Seismic behavior of hinged steel frames with masonry infill walls. J Build Eng 2023;vol. 77:107536. https://doi.org/10.1016/j.jobe.2023.107536.
[4] Mattei F, Giuliani G, Andreotti R, Caprili S, Tondini N. Experimental and numerical assessment of a steel frame equipped with dissipative replaceable bracing connections. Presente Procedia Struct Integr 2022:1204–11. https://doi.org/10.1016/j.prostr.2023.01.155.
[5] De Angelis A, Pecce MR. The structural identification of the infill walls contribution in the dynamic response of framed buildings. Struct Control Health Monit 2019; vol. 26(9). https://doi.org/10.1002/stc.2405.
[6] Morelli F, Natali A, Poggi G. Seismic behavior and nonlinear analysis of hybrid coupled shear walls. Procedia Struct Integr 2023;vol. 44:574–81. https://doi.org/10.1016/j.prostr.2023.01.075.
[7] Dolšek M, Fajfar P. The effect of masonry infills on the seismic response of a four-storey reinforced concrete frame — a deterministic assessment. Eng Struct 2008; vol. 30(7). https://doi.org/10.1016/j.engstruct.2008.01.001.
[8] Nicola T, Leandro C, Guido C, Enrico S. Masonry infilled frame structures: state-of-the-art review of numerical modelling. Earthq Struct 2015;vol. 8(3). https://doi.org/10.12989/EAS.2015.8.3.733.
[9] Di Sarno L, Paolacci F, Sextos AG. Seismic performance assessment of existing steel buildings: a case study. Key Eng Mater 2018;vol. 763:1067–76. https://doi.org/10.4028/www.scientific.net/KEM.763.1067.
[10] Mucedero G, Perrone D, Brunesi E, Monteiro R. Numerical modelling and validation of the response of masonry infilled RC frames using experimental testing results. Buildings 2020;vol. 10(10). https://doi.org/10.3390/buildings10100182.
[11] Dias-Oliveira J, Rodrigues H, Asteris PG, Varum H. On the Seismic Behavior of Masonry Infilled Frame Structures. Buildings 2022;vol. 12(8). https://doi.org/10.3390/buildings12081146.
[12] Su Q, Cai G, Hani M, Si Larbi A, Tsavdaridis KD. Damage control of the masonry infills in RC frames under cyclic loads: a full-scale test study and numerical analyses. Bull Earthq Eng 2023;vol. 21(2). https://doi.org/10.1007/s10518-022-01565-y.
[13] Zahrai SM, Moradi A, Moradi M. Using friction dampers in retrofitting a steel structure with masonry infill panels. Steel Compos Struct 2015;vol. 19(2).
[14] Gara F, Arezzo D, Nicoletti V, Carbonari S. Monitoring the modal properties of an RC school building during the 2016 central Italy seismic swarm. J Struct Eng 2021; vol. 147(7):05021002. https://doi.org/10.1061/(ASCE)ST.1943-541X.0003025.
[15] Furtado A, Rodrigues H, Arêde A, Varum H. Modal identification of infill masonry walls with different characteristics. Eng Struct 2017;vol. 145:118–34. https://doi.org/10.1016/j.engstruct.2017.05.003.
[16] Nicoletti V, Arezzo D, Carbonari S, Gara F. Vibration-based tests and results for the evaluation of infill masonry walls influence on the dynamic behaviour of buildings: a review. Arch Comput Methods Eng Oct. 2022;vol. 29(6):3773–87. https://doi.org/10.1007/s11831-022-09713-y.
[17] Varum H, Furtado A, Rodrigues H, Dias-Oliveira J, Vila-Pouca N, Arêde A. Seismic performance of the infill masonry walls and ambient vibration tests after the Ghorka 2015, Nepal earthquake. Bull Earthq Eng 2017;vol. 15(3):1185–212. https://doi.org/10.1007/s10518-016-9999-z.
[18] Nicoletti V, Arezzo D, Carbonari S, Gara F. Expeditious methodology for the estimation of infill masonry wall stiffness through in-situ dynamic tests. Constr Build Mater 2020;vol. 262:120807. https://doi.org/10.1016/j.conbuildmat.2020.120807.
[19] De Angelis A, Pecce MR. Out-of-plane structural identification of a masonry infill wall inside beam-column RC frames. Eng Struct 2018;vol. 173:546–58. https://doi.org/10.1016/j.engstruct.2018.06.072.
[20] Agante M, Furtado A, Rodrigues H, Arêde A, Fernandes P, Varum H. Experimental characterization of the out-of-plane behaviour of masonry infill walls made of lightweight concrete blocks. Eng Struct 2021;vol. 244:112755. https://doi.org/10.1016/j.engstruct.2021.112755.
[21] De Angelis A, Bilotta A, Pecce MR, Pollastro A, Prevete R. Dynamic identification methods and artificial intelligence algorithms for damage detection of masonry

infills. J Civ Struct Health Monit 2024;vol. 14(6). https://doi.org/10.1007/s13349-024-00790-0.
[22] Mohamed H, Furtado A, Rodrigues H. Appraisal of masonry infill walls dynamic characteristics: an analytical study. Eng Struct 2023;vol. 297:116995. https://doi.org/10.1016/j.engstruct.2023.116995.
[23] Nicoletti V, Arezzo D, Carbonari S, Gara F. Detection of infill wall damage due to earthquakes from vibration data. Earthq Eng Struct Dyn 2023;vol. 52(2). https://doi.org/10.1002/eqe.3768.
[24] C. Conti, 'Université de Mons EASYMOD: A MATLAB/SCILAB TOOLBOX FOR TEACH- ING MODAL ANALYSIS', Accessed: Aug. 07, 2024. [Online]. Available: ⟨https://www.academia.edu/31671411/Universit%C3%A9_de_Mons_EASYMOD_A_MATLAB_SCILAB_TOOLBOX_FOR_TEACH_ING_MODAL_ANALYSIS⟩.
[25] 'Modal Testing: Theory, Practice and Application, 2nd Edition | Wiley'. Accessed: Aug. 07, 2024. [Online]. Available: ⟨https://www.wiley.com/en-us/Modal+Testing%3A+Theory%2C+Practice+and+Application%2C+2nd+Edition-p-9780863802188⟩.
[26] 'SAP+MATLAB'. Accessed: Jun. 17, 2024. [Online]. Available: ⟨https://it.mathworks.com/matlabcentral/fileexchange/79271-sap-matlab⟩.
[27] R.J. Allemang and D.L. Brown, 'A Correlation Coefficient for Modal Vector Analysis', presented at the Proceedings of the 1st International Modal Analysis Conference (IMAC I), Orlando, Nov. 1982, pp. 110–116.